Morphological control of band offsets for transparent bipolar hetero-junctions: The Bädeker Diode

Keith T. Butler [*,1]

[1]Centre for Sustainable Chemical Technologies and Department of Chemistry, University of Bath, Claverton Down, Bath, BA2 7AY, UK

Received ZZZ, revised ZZZ, accepted ZZZ
Published online ZZZ (Dates will be provided by the publisher.)

Keywords Bipolar hetero-junction, band-alignment, DFT, Cuprous Iodide

* Corresponding author: e-mail k.t.butler@bath.ac.uk, Phone: +44 (0)1225 388388, Fax: +44(0) 1225 386231

Cuprous iodide is an important transparent p-type semiconductor, it has an illustrious history and has recently enjoyed a renaissance. In this work we investigate the electronic band structure and absolute electron energies of the three major known phases of CuI, zincblende (*F43m*), wurtzite (*P63mc*) and rock salt (*Fm-3m*). We also consider CdO, an important n-type transparent semiconductor in these three phases, in order to assess the possibility of constructing transparent bipolar hetero-junctions from the two materials. We calculate the relative stability of all three phases of both materials, demonstrating that all three phases should be accessible through non-equilibrium growth techniques. We then calculate the band structures of all six phases, as well as the absolute electron energies (ionisation potentials and electron affinities). Thus, we are able to construct energy band alignment diagrams between the materials in the three different structures. These diagrams reveal that one can achieve type-I, type-II or type-III offsets depending on the crystal structure of the materials. We consider possible applications opened up by these findings.

1 Introduction

Cuprous iodide (CuI) occupies a privileged place in semiconductor history as the first intentionally doped conductor; Karl Bädeker first observed a positive Hall coefficient whilst measuring the conductivity of samples he had produced[1]. It took several years and the contribution of scientific luminaries such as Werner Heisenberg[2] and Robert Peierles[3] before the full meaning of Bädeker's measurements - the first observation of conductivity mediated by holes (p-type) - became apparent. This historical importance alone would make CuI an important material, but there's much more to CuI than this.

The property of being a transparent p-type semiconductor also places CuI in a particularly important position from a technological perspective. Bipolar (p-n) semiconductor hetero-junctions are basis of a staggering amount of today's technology[4,5], the ability to produce fully transparent p-n hetero-junctions opens up wide new areas of technological application[6–8], providing electronic devices which do not impinge on the operation and aesthetics of their environment. Transparent semiconductors with n-type (electron conducting) character are well known and the transparent conductive oxides (TCOs) represent one of the greatest areas of materials' development in the past decades. However, the development of p-type transparent conductors has been far more difficult, examples such as NiO[9,10] and CuAlO[11] are known. Nonetheless, the quest for p-type transparent conductors continues apace to this day, with the full arsenal of cutting edge experimental[12,13] and theoretical techniques[14–18] being employed in the search.

The problem is that stabilisation of a hole in the valence band of a material requires that that material have relatively small ionisation potential – placing the valence band maximum (VBM) close to the vacuum level, whilst optical transparency generally requires a wide band gap (> 2.5 eV). The result of these predicates is that the conduction band minimum (CBM) must be even closer to the vacuum level. This set of necessary conditions for p-type transparent conductors is seldom fulfilled in traditional oxide transparent semiconductors.

Table 1 Assorted energetic and electronic properties of the zincblende, wurtzite and rock salt phases of CuI and CdO. The energy difference from the ground state phase per formula unit (ΔE), the direct band gap (Eg dir), the indirect band gap (Eg ind), the ionisation potential (IP) and electron affinity (EA).

Species	Phase	ΔE (eV)	Eg(dir) (eV)	Eg(ind) (eV)	IP (eV)	EA (eV)
CuI	*ZB*	0.00	2.43	2.43	5.80	3.37
	WZ	0.00	3.02	3.02	5.20	2.18
	RS	0.39	2.28	0.68	5.30	4.62
CdO	*ZB*	0.15	3.12	3.12	6.31	3.19
	WZ	0.11	0.98	0.98	6.46	5.48
	RS	0.00	2.03	0.78	6.02	5.24

Recently, however, reports of functioning transparent p-n hetero-junctions based on a CuI/ZnO architecture have emerged[19,20]. These papers report highly rectifying junctions with type-II band offset. These junctions are reported to have ideality factors greater than 2, which have been attributed to the fact that current flow across the interface occurs via recombination of carriers (electrons and holes) at the junction. Such type-II offset junctions have several important technological applications, including photodetectors and field-effect transistors. Additionally they have been mooted as possible materials for transparent photovoltaics, although we feel that the twin properties of light to energy conversion and transparency to be somewhat contradictory.

CdO is another transparent conductor first reported by Bädeker[21], unlike CuI it displays 'regular' Hall behaviour, with a negative coefficient and electron mediated transport. It occurs naturally in the rock-salt (*Fnma*) structure and is recognised as a useful n-type transparent semiconductor. CdO has been heavily studied in recent years, both experimentally[22,23] and theoretically[24,25], due to its intrinsic interest and technological relevance. The former includes an indirect band gap and large Moss-Burstein[24] shift in the energy transitions, the latter includes, in particular, application in light emitting diodes[26].

Although CdO and CuI have different ground state phases both have known structures in the other's ground state configuration, i.e. rock salt CuI and zincblende CdO are known structures. With the advent of non-equilibrium growth techniques this presents the intriguing possibility of a 'Bädeker diode' comprised of either rock salt, zincblende or indeed wurtzite hetero-junctions of these materials. In this contribution we show that the junction can display any of type-I , type-II or type–III band offsets. Such configurations could be of great utility as outlined above and in a range of other important technological applications as discussed in § 3.4. The question remains as to whether such a junction is feasible and exactly what type of band structure it would display. Computational modelling, based on density functional theory (DFT) provides a way to answer these questions without recourse to expensive experimental investigations

2 Computational methods

All calculations in this study were performed using the VASP package [27], within the projector augmented wave formalism[28,29]. The structures were optimised using the PBE-Sol functional [30], with a plane-wave cutoff energy of 500 eV and k-point mesh sampling defined as an evenly spaced grid in reciprocal space with a density scaled to the unit cell size to achieve uniform sampling with a target length cutoff of 1 nm, as described by Moreno and Soler[31]. Using the vacuum level of the various materials and phases as an absolute reference we align the band edges. The reference energy level for the valence band maximum (VBM) is then the ionisation potential (IP), the conduction band minimum (CBM) is calculated as IP + band gap (E_g). IP is defined as the difference between vacuum electrostatic potential (V_{vac}) and the VBM in the slab. As the VBM in the slab calculation is affected by nascent states induced by the surface, we calculate the VBM of the material by reference to a bulk calculation. The bulk calculation of band edge position is performed using the hybrid HSE06 functional[32]. This means that in addition to removing the nascent surface states, this correction also accounts for the shift in band edges from the exact treatment of electron correlation. This method for solid and porous materials is described in greater detail elsewhere[33–35]. All required properties are acquired by processing of the electrostatic potential from the DFT calculations using the MacroDensity package, which is freely available with examples and tutorials[36].

3 Results

3.1 Phase stability The total energies of the phases of CuI and CdO are presented in table 1. The energies demonstrate that the wurtzite and zincblende phases of CuI are almost degenerate energetically, actually the DFT calculation predicts that the zincblende phase is slightly more energetically favourable than the wurtzite phase (4 meV), which matches the observation that zincblende is the low temperature ground state. The rock salt phase is significantly more energetically unfavourable, the preference for tetrahedral (zincblende/wurtzite) structures over octahedral can be understood as arising from the ratios of the ionic radii of the species[37].

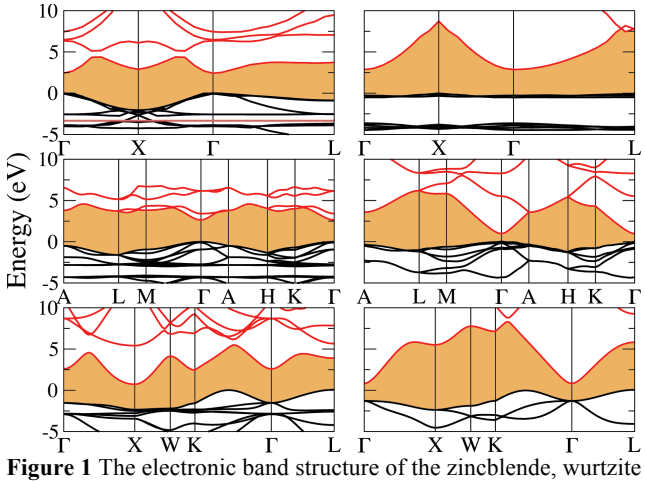

Figure 1 The electronic band structure of the zincblende, wurtzite and rock salt phases of CuI and CdO. Left column CuI, right column CdO. Phases from top to bottom, zincblende, wurtzite, rock salt. The VBM is set to zero, valence bands are jet black, conduction bands are crimson, and the band gap is golden brown.

Conversely CdO is well known to prefer the rock salt structure, also in line with the calculated energies of the phases. Although both materials have a preference for different phases, the energetic difference between the phases is sufficiently small that it may be possible to grow commensurate phases of one on the other by means of epitaxy. To further explore the potential properties of such a structure we now turn to the electronic structure of the phases.

3.2 Bulk electronic structure: The bulk electronic band structures are plotted in figure 1. Both species are direct band gap semiconductors in the tetragonal phases (zincblende and wurtzite) and indirect gap semiconductors in the rock salt phase. In the zincblende phase both CuI and CdO are transparent with band gaps of 2.43 and 3.12 respectively. Note that in our simulations we use the HSE06 hybrid functional with 25 % of exact Hartree-Fock exchange, this probably leads to an under-estimation of the band-gap in CuI, due to the overestimation of long-range exchange screening. This explains the fact that the band gap for CuI is underestimated by around 0.6 eV with respect to experimental values.

In the wurtzite phase the two materials show opposite trends. CdO has a rather narrow gap (0.98 eV) at the Gamma point, whereas CuI has a wider gap than in zincblende, by around 0.6 eV. The opposite trends can be interpreted by considering the bonding contributions to the VBM. In CuI the VBM is comprised of Cu *d* and I *p* orbitals which are hybridised. In the wurtzite structure the atoms are closer together, thus the hybridisation is stronger. This leads to greater stabilisation of the VBM with respect to the CBM. This is the classic behaviour displayed by tetrahedral semiconductors[38]. In the CdO structures the VBM is comprised solely of O *p* states, so there is no hybridisation, consequently no opening up of the band gap. Rather, the increased kinetic energy caused by the reduction in the interatomic distance leads to band broadening and a reduced gap.

In the rock salt phase the direct and indirect band gaps of CdO are 2.03 and 0.78 eV respectively, in good agreement with experimental and previously calculated values[24]. In CuI the gaps are similar 2.28 and 0.68 eV for direct and indirect gaps.

3.3 Absolute electron energies: We now turn our attention to the calculated electronic energies of the slab models. For all structures surface cuts with zero net dipole were constructed using the METADISE program[39]. This choice ensures no macroscopic electric field across the slab model. For rock salt structures the (001) surface was used, for wurtzite and zincblende the (110) surfaces were used.

The calculated electron energies - IPs and electron affinities (EAs) - are presented in table 1. The electron energies for CuI are consistently closer to the vacuum level than those in CdO. This can be understood from the Madelung potential[40] of the ionic sites. The Madelung potential expresses the energy required to remove an ion from its site in a crystal lattice, this means that it also corresponds to the amount by which the ion is stabilised by the electrostatic environment of the crystal. The electrostatic potential is the leading order term in determining the stability of an electron in a solid (further terms such as kinetic and exchange-correlation energy also contribute), therefore it is a good indicator of the IP and EA. CuI is comprised of +/- 1 formally charged ions, whist CdO is comprised of +/- 2 formally charged ions. Therefore the Madelung potential is far greater in the CdO lattice. The relative values of the IP and EA also explain why CuI is p-type, whilst CdO is n-type. The greater the Madelung potential and hence the EA the greater is the stabilisation energy of an excess electron in the lattice.

With the series of CuI phases the trends in IP and EA are subject to a more subtle interplay of factors. The bond length determines the strength of individual electrostatic interactions, whilst the crystal structure determines the number of such interactions in the first sphere of the ion. Shorter bond lengths however also contribute to higher kinetic energy of electrons and hence band broadening. As such it is difficult to predict *a priori* which of the phases will have the largest IPs and EAs. Interestingly the ground state of CuI has the greatest IP whilst the ground state of CdO has the smallest IP, demonstrating the difficulty in predicting the IPs from simple electrostatic arguments.

3.4 Band alignments With knowledge of the electron energies on an absolute scale we can now construct energy band alignment diagrams for the different phases, predicting the offsets in the energy levels if epitaxial hetero-structures were produced. We note that the offsets predicted here are first approximations to those a real hetero-structure, where the effects of strain (deformation potential [38,41–43]) and interface dipoles[33,44–46] would also play an important role. Nonetheless, the offsets from the single phases are the dominant contribution and the calculated offsets

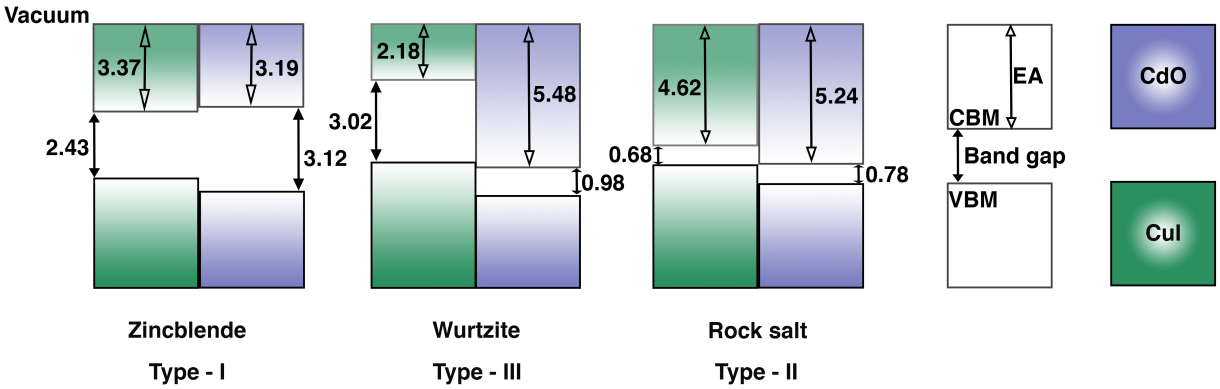

Figure 2 The energy band alignment diagrams of the zincblende, wurtzite and rock salt phases of CuI and CdO. The structure type and band alignment classification are given below each diagram, a key to the various quantities is given on the right.

highlight the ability to design different interface types by changing the crystal phases, with each crystal structure displaying a different type of offset.

The zincblende junction displays the straddled gap type- I band offsets. The IP of CdO is greater and the EA of CdO is smaller than the corresponding values in CuI. This arrangement of electron energies means that excitons in such a system would be confined to the CuI system. This type of offset is often applied in core-shell structures for fluorescence.

The wurtzite junction has a broken gap type-III offset. The energy IP of CuI is smaller than the EA of CdO. This results in a spontaneous flow of electrons from the CuI valence band to the CdO conduction band, forming a metallic interface and compensating space charge regions in the materials, to maintain charge neutrality. This type of offset has been predicted to lead to high frequency operation at low voltages, as such it could be applied in various power constrained scenarios including implantable medical applications and ultra-mobile computing technologies [47].

The rock salt structure has type-II staggered offset with the IP and EA of CdO greater than in CuI. This type of staggered offset is useful in applications where charge separation is required. Holes are stabilised in CuI and electrons in CdO, this is similar to the offset in CuI/ZnO junctions, which display high rectification[48].

4 Conclusions We have considered the zincblende, wurtzite and rock salt phases of CuI and CdO. Comparison of total internal energies demonstrates that all three phases in both materials are either stable or meta-stable, meaning that any of the phases should be accessible through equilibrium or non-equilibrium growth techniques.

We considered the electronic structure of each of these phases, explaining the differences in observed trends upon phase transition by considering the hybridisation of the electronic states which constitute the valence band edge. CuI is found to display the behaviour expected of tetrahedral semiconductors, due to the *p-d* hybrid nature of the VBM. In CdO where the band edge is almost purely O *p* in character kinetic band broadening effects dominate.

We calculate the absolute electron energies of the band edges with respect to the vacuum level, thus allowing us to construct energy band alignment diagrams for all three crystal structures. The diagrams reveal that zincblende has a type-I offset, wurtzite has a type-III offset and rock salt has a type-II offset. Finally we propose possible technological applications of interest given these band offset configurations.

Acknowledgements M. Hoff, C. Holman Hendon, ULTRAFOX.

References

(1) Bädeker, K. *Ann. Phys.* **1909**, *334*, 566–584.

(2) Heisenberg, W. *Ann. Phys.* **1931**, *402*, 888–904.

(3) Peierls, R. *Zeitschrift f*[illegible]*r Phys.* **1929**, *53*, 255–266.

(4) Kroemer, H.; Griffiths, G. *IEEE Electron Device Lett.* **1983**, *4*, 20–22.

(5) Herbert Kroemer - Nobel Lecture: Quasi-Electric Fields and Band Offsets: Teaching Electrons New Tricks http://www.nobelprize.org/nobel_prizes/physics/laureates/2000/kroemer-lecture.html (accessed Dec 22, 2014).

(6) Kudo, A.; Yanagi, H.; Ueda, K.; Hosono, H.; Kawazoe, H.; Yano, Y. *Appl. Phys. Lett.* **1999**, *75*, 2851.

(7) Tate, J.; Jayaraj, M. K.; Draeseke, A. D.; Ulbrich, T.; Sleight, A. W.; Vanaja, K. A.; Nagarajan, R.;

Wager, J. F.; Hoffman, R. L. *Thin Solid Films* **2002**, *411*, 119–124.

(8) Wager, J. F. *Thin Solid Films* **2008**, *516*, 1755–1764.

(9) Sato, H.; Minami, T.; Takata, S.; Yamada, T. *Thin Solid Films* **1993**, *236*, 27–31.

(10) Irwin, M. D.; Buchholz, D. B.; Hains, A. W.; Chang, R. P. H.; Marks, T. J. *Proc. Natl. Acad. Sci.* **2008**, *105*, 2783–2787.

(11) Kawazoe, H.; Yasukawa, M.; Hyodo, H.; Kurita, M.; Yanagi, H.; Hosono, H. **1997**, *389*, 939–942.

(12) Quackenbush, N. F.; Allen, J. P.; Scanlon, D. O.; Sallis, S.; Hewlett, J. A.; Nandur, A. S.; Chen, B.; Smith, K. E.; Weiland, C.; Fischer, D. A.; Woicik, J. C.; White, B. E.; Watson, G. W.; Piper, L. F. J. *Chem. Mater.* **2013**, *25*, 3114–3123.

(13) Sallis, S.; Piper, L. F. J.; Francis, J.; Tate, J.; Hiramatsu, H.; Kamiya, T.; Hosono, H. *Phys. Rev. B* **2012**, *85*, 085207.

(14) Scanlon, D. O.; Walsh, A.; Watson, G. W. *Chem. Mater.* **2009**, *21*, 4568–4576.

(15) Hautier, G.; Miglio, A.; Waroquiers, D.; Rignanese, G.-M.; Gonze, X. *Chem. Mater.* **2014**, *26*, 5447–5458.

(16) Varley, J. B.; Lordi, V.; Miglio, A.; Hautier, G. *Phys. Rev. B* **2014**, *90*, 045205.

(17) Hautier, G.; Miglio, A.; Ceder, G.; Rignanese, G.-M.; Gonze, X. *Nat. Commun.* **2013**, *4*, 2292.

(18) Robertson, J.; Clark, S. J. *Phys. Rev. B* **2011**, *83*, 075205.

(19) Schein, F.-L.; von Wenckstern, H.; Grundmann, M. *Appl. Phys. Lett.* **2013**, *102*, 092109.

(20) Grundmann, M.; Karsthof, R.; von Wenckstern, H. *ACS Appl. Mater. Interfaces* **2014**, *6*, 14785–14789.

(21) Bädeker, K. *Ann. Phys.* **1907**, *327*, 749–766.

(22) Piper, L.; Colakerol, L.; King, P.; Schleife, A.; Zúñiga-Pérez, J.; Glans, P.-A.; Learmonth, T.; Federov, A.; Veal, T.; Fuchs, F.; Muñoz-Sanjosé, V.; Bechstedt, F.; McConville, C.; Smith, K. *Phys. Rev. B* **2008**, *78*, 165127.

(23) Mudd, J. J.; Lee, T.-L.; Muñoz-Sanjosé, V.; Zúñiga-Pérez, J.; Hesp, D.; Kahk, J. M.; Payne, D. J.; Egdell, R. G.; McConville, C. F. *Phys. Rev. B* **2014**, *89*, 035203.

(24) Burbano, M.; Scanlon, D. O.; Watson, G. W. *J. Am. Chem. Soc.* **2011**, *133*, 15065–15072.

(25) Schleife, A.; Rödl, C.; Fuchs, F.; Furthmüller, J.; Bechstedt, F. *Phys. Rev. B* **2009**, *80*, 035112.

(26) Yu, K. M.; Mayer, M. A.; Speaks, D. T.; He, H.; Zhao, R.; Hsu, L.; Mao, S. S.; Haller, E. E.; Walukiewicz, W. *J. Appl. Phys.* **2012**, *111*, 123505.

(27) Kresse, G.; Furthmüller, J. *Comput. Mater. Sci.* **1996**, *6*, 15–50.

(28) Blöchl, P. E. *Phys. Rev. B* **1994**, *50*, 17953–17979.

(29) Kresse, G. *Phys. Rev. B* **1999**, *59*, 1758–1775.

(30) Perdew, J.; Ruzsinszky, A.; Csonka, G.; Vydrov, O.; Scuseria, G.; Constantin, L.; Zhou, X.; Burke, K. *Phys. Rev. Lett.* **2008**, *100*, 136406.

(31) Moreno, J.; Soler, J. *Phys. Rev. B* **1992**, *45*, 13891–13898.

(32) Heyd, J.; Scuseria, G. E.; Ernzerhof, M. *J. Chem. Phys.* **2006**, *124*, 219906.

(33) Peressi, M.; Binggeli, N.; Baldereschi, a. *J. Phys. D. Appl. Phys.* **1998**, *31*, 1273–1299.

(34) Alkauskas, A.; Broqvist, P.; Devynck, F.; Pasquarello, A. *Phys. Rev. Lett.* **2008**, *101*, 106802.

(35) Butler, K. T.; Hendon, C. H.; Walsh, A. *J. Am. Chem. Soc.* **2014**, *136*, 2703–2706.

(36) MacroDensity https://github.com/WMD-Bath/MacroDensity (accessed Jan 2, 2015).

(37) Pauling, L. *J. Am. Chem. Soc.* **1929**, *51*, 1010–1026.

(38) Li, Y.-H.; Gong, X.; Wei, S.-H. *Phys. Rev. B* **2006**, *73*, 245206.

(39) Watson, G. W.; Oliver, P. M.; Parker, S. C. *Phys. Chem. Miner.* **1997**, *25*, 70–78.

(40) Born, M.; Huang, K. *Dynamical Theory of Crystal Lattices*; Clarendon Press, 1998; p. 420.

(41) Łepkowski, S. P.; Gorczyca, I.; Stefańska-Skrobas, K.; Christensen, N. E.; Svane, a. *Phys. Rev. B* **2013**, *88*, 081202.

(42) Butler, K. T.; Hendon, C. H.; Walsh, A. *ACS Appl. Mater. Interfaces* **2014**, *6*, 22044–22050.

(43) Hinuma, Y.; Oba, F.; Kumagai, Y.; Tanaka, I. *Phys. Rev. B* **2012**, *86*, 245433.

(44) Walsh, A.; Butler, K. T. *Acc. Chem. Res.* **2014**, *47*, 364–372.

(45) Butler, K. T.; Buckeridge, J.; Catlow, C. R. A.; Walsh, A. **2014**, *115320*, 1–6.

(46) Long, W.; Li, Y.; Tung, R. T. *Thin Solid Films* **2013**, 4–6.

(47) Li, W.; Zhang, Q.; Bijesh, R.; Kirillov, O. A.; Liang, Y.; Levin, I.; Peng, L.-M.; Richter, C. A.; Liang, X.; Datta, S.; Gundlach, D. J.; Nguyen, N. V. *Appl. Phys. Lett.* **2014**, *105*, 213501.

(48) Grundmann, M.; Karsthof, R.; von Wenckstern, H. *ACS Appl. Mater. Interfaces* **2014**, *6*, 14785–14789.